Journal of Magnetism and Magnetic Materials 93 (1991) 109–115
North-Holland

Invited paper

Scanning Electron Microscopy with Polarization Analysis (SEMPA) – studies of domains, domain walls and magnetic singularities at surfaces and in thin films

M.R. Scheinfein, J. Unguris, M. Aeschlimann[1], D.T. Pierce and R.J. Celotta
National Institute of Standards and Technology, Gaithersburg, MD 20899, USA

Scanning Electron Microscopy with Polarization Analysis (SEMPA) is used to investigate the surface magnetic microstructure of domain walls in thin permalloy films and the domain structure of magneto-optic TbFeCo alloys. Domain wall measurements confirm the results of micromagnetic theory.

1. Introduction

Over the past several years scanning electron microscopy with polarization analysis (SEMPA) has matured enough that it can now obtain quantitative high resolution surface magnetization maps of ferromagnetic [1–7] and ferrimagnetic surfaces [8]. From such measurements high spatial resolution images can be obtained of surface domains, domain walls and magnetic topological singularities. In addition to answering fundamental questions about magnetic microstructure, information gained from such studies can assist researchers involved in developing new families of higher density magnetic storage media.

SEMPA is one of many techniques used for microstructural characterization of magnetic materials. In SEMPA a finely focused beam of medium energy (5–50 keV) electrons is rastered across a sample. Secondary electrons are excited near the surface by the focused electron beam. The secondary electrons emitted from the surface of a sample maintain their spin orientation. The net polarization of the emitted secondary electrons is directly related to the sample magnetization for ferromagnetic materials [9]. In ferrimagnetic materials, as we will show, the spin polarized secondary electrons originate primarily in the transition metal subnetwork [8]. Surface magnetization maps are generated at high spatial resolution by spin analyzing the emitted polarized secondary electrons point-by-point as the incident beam rasters across the sample surface. The information gained from a SEMPA experiment elucidates the micromagnetic structure close to the surface (< 1–5 nm).

In this paper we will use SEMPA to show the influence of the surface on 180° domain wall microstructure [3, 5, 10]. We will focus on the regime where film thickness plays a critical role in determining the wall magnetic microstructure. Finally, examples from magneto-optic recording will be used to show the effects of thin segregation layers on magnetic microstructure near the surface.

2. 180° domain walls in permalloy

In a bulk material, 180° degree Bloch walls are formed in the interior of the ferromagnet, while Néel type walls are formed at the surfaces. The penetration of the Néel wall into the bulk is on

[1]Present address: Center for Photoinduced Charge Transfer, Department of Chemistry, University of Rochester, Rochester, NY 14627, USA.

the order of a Bloch wall width for bulk samples [5, 10]. For all but the highest anisotropy materials, this Néel wall penetration is on the order of tens of nanometers or larger. The structure of domain walls in thin films can be very different from that of semi-infinite systems. As the thickness of the film approaches approximately three Bloch wall widths, a vortex-like structure forms within the film. This vortex wall structure is called an asymmetric Bloch wall, a term coined by LaBonte [11].

We calculate the micromagnetic structure present in domain walls by following the methods used by Brown [12], LaBonte [11], Hubert [13] and Aharoni [14]. The equilibrium configuration of domain walls in ferromagnetic materials results from a minimization of a system's total magnetic energy. The system's total energy is composed of the mean field exchange, bulk magnetocrystalline anisotropy, surface magnetocrystalline anisotropy, self-magnetostatic and external magnetostatic energies. We solve for the magnetization distribution in a domain wall by considering a boundary value problem in two spatial dimensions with the constraint of constant magnetization [10–14]. The minimum energy state is found iteratively.

The calculated cross section of an asymmetric Bloch wall in a 160 nm thick permalloy film is shown in fig. 1a. The magnetization is out of the page to the left of the wall $(-y)$ and into the page to the right of the wall $(+y)$. The uniaxial easy axis of magnetization is along the y-axis. The hard axis components of the magnetization, M_x and M_z, are shown in the figure. The micromagnetics simulation is performed with a nearest neighbor exchange parameter of 1.05×10^{-6} erg/cm, a uniaxial anisotropy which includes magnetostriction of 1743 erg/cm^3 and a saturation magnetization of 813 emu/cm^3. No special surface anisotropy was included in this simulation. The vortex structure in the asymmetric Bloch wall is clearly evident in fig. 1a. The size of the vortex structure is a sensitive function of thickness for films in the asymmetric Bloch wall thick-

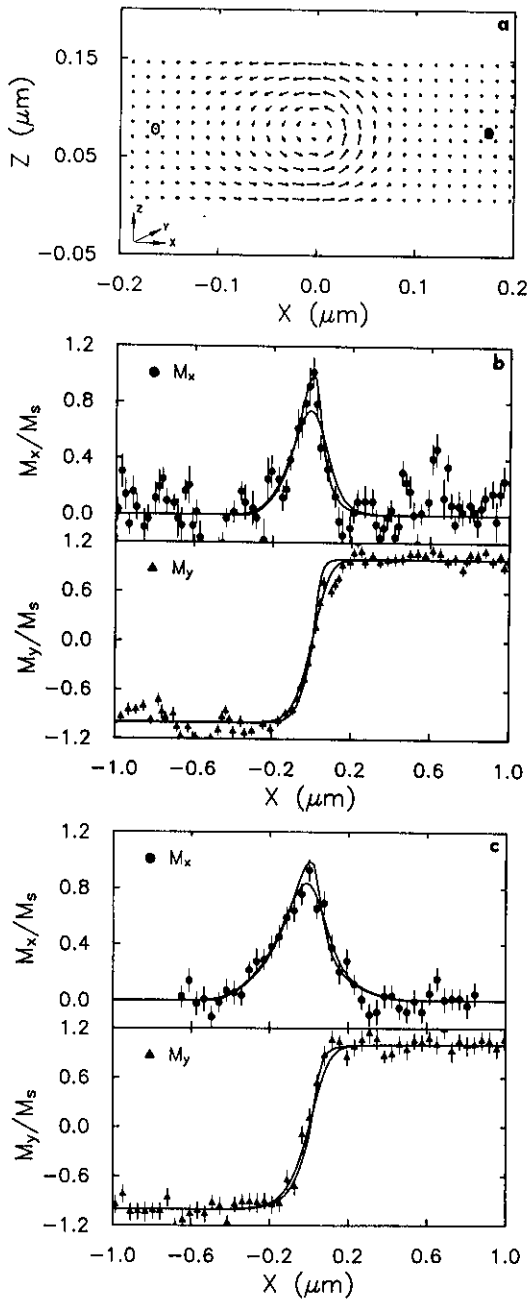

Fig. 1. (a) Cross section of the hard-axis magnetization directions in a 160 nm thick permalloy film; (b) surface magnetization profiles for a 160 nm thick and (c) 240 nm thick permalloy film. The solid symbols are the experimental data. The solid lines are the unconvoluted micromagnetic calculation results (upper curve in each panel) and the micromagnetic calculation results convolved with a 110 nm probe (lower curve in each panel).

ness regime. In the SEMPA experiment we are sensitive to the surface magnetization. This is equivalent to sampling the top-most layer of discretized cells in the calculated magnetization profile in a domain wall.

Surface domain wall magnetization profiles are shown in figs. 1b and c for two different thicknesses of permalloy. The solid symbols represent the experimental wall magnetization data from a 160 nm thick permalloy film in fig. 1b. The solid lines are the results of micromagnetic simulations. The upper solid line depicts the calculated x-component of the magnetization whereas the lower solid line has the calculated result convolved with an instrument function which corrects for the finite resolution of a 110 nm probe. The 110 nm convolution process sets the upper limit of the probe size effect and was assessed experi-

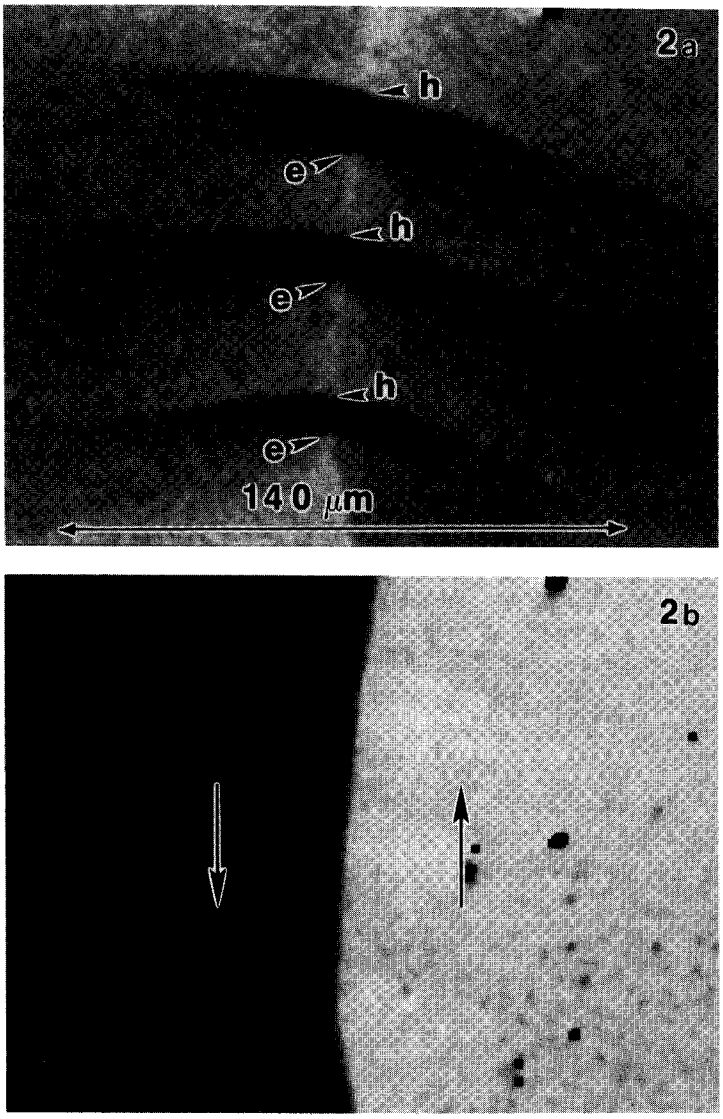

Fig. 2. (a) X-component and (b) y-component of the magnetization in cross-tie walls in a 40 nm thick permalloy film.

mentally for the conditions under which these data were collected. The y-component of the magnetization is along the domain easy axis directions. No out-of-plane (z-component) magnetization was found. The solid symbols in fig. 1c represent the experimental wall magnetization data from a 240 nm thick permalloy film. The solid lines are once again the results of the unconvolved micromagnetic simulation and simulation results convolved with a 110 nm probe function. The total RMS deviations of the experimental data from the calculated data are less than 0.15 and 0.11 for the 160 and 240 nm films, respectively [10]. The full width at half maximum of M_x is roughly equal to the film thickness.

As the film thickness is decreased further, the asymmetric Bloch wall structure degenerates into a pure Néel wall. However, in the transition thickness between an asymmetric Bloch wall and a Néel wall, cross-tie walls are formed. The x- and y-components of the magnetization in a cross-tie wall in a 40 nm thick permalloy film are shown in figs 2a and b. The easy axis of magnetization is along the y-axis as evidenced by the two well formed domains in fig. 2b. The thin white line between the domains in fig. 2a is the Néel wall part of the cross-tie wall. The large triangular shapes are the cross-ties themselves. These are formed by a complicated interaction of two magnetic singularities which are located close to one another. In any two-dimensional plane the vector magnetization may form singularities of either the elliptical or hyperbolic type. An elliptical singularity is located at the point of the cross-tie triangle which is denoted by an "e" in fig. 2a. The magnetization rotates counterclockwise about the singularity. A hyperbolic singularity is located at the intersection of the wall and the flat part of the cross-tie triangle which is denoted by an "h" in fig. 2a. The magnetization forms hyperbolic loci about this singularity. The z-component of the singularity is spatially too small to detect with our current SEMPA apparatus, as the diameter of the singularity should be on the order of 20 nm. However, it is likely that the orientation of the z-component of the magnetization within these singularities has opposite orientation for the elliptical and hyperbolic cases [15]. The two singularities are coupled together by their dipolar magnetic fields thus forming the cross-tie structure. Interestingly, this perturbation of the singularities is propagated several microns away from the wall and into the domains.

3. Domains in thin magneto-optic films

Magneto-optic materials such as TbFeCo alloys are used for the thermomagnetic writing of bits for data storage. These alloys exhibit a large perpendicular magnetocrystalline anisotropy which make them excellent candidates for perpendicular recording material [16, 17]. Of the strategies for recording magnetic information in perpendicular media using higher data transfer rates, direct overwrite magneto-optic disk technology has been the target of extensive research [18, 19] with one of the most promising techniques being magnetic-field modulation (MFM) [20, 21]. In this method, the magneto-optic layer is heated continuously by a laser beam while an externally applied magnetic field, which is modulated at high frequency, switches the bit orientations. Characteristic crescent shaped domains of variable length are the result of this MFM thermomagnetic writing process. SEMPA measurements of the written bits were made in order to characterize the size and shape of the domains and any irregularities in the domain boundaries as a function of the material composition and applied switching field intensity.

Lorentz transmission electron microscopy (TEM) can be used to examine magnetic domain microstructure [17] at high spatial resolution in thin films, but contrast can be low for ferrimagnetic systems near the compensation temperature. Near the compensation temperature, the saturation magnetization is nearly zero, and the

resultant magnetic fields in and near the sample are small. Hence, the net Lorentz TEM contrast can be extremely small. This is the case for magnet-optic recording materials at room temperature. However, we will show that in the SEMPA measurements, the contrast can still be quite high for magnetically compensated materials.

We have characterized different compositions of $Tb_xFe_yCo_{1-x-y}$ alloys at different (writing) applied fields using SEMPA and TEM Lorentz [8, 17]. The films were prepared by three gun electron beam evaporation [21] onto Si/Si_3N_4 substrates with Si_3N_4 thin film windows. The magneto-optic layer was protected from corrosion by a 10 nm Al layer and a 25 nm SiO_2 overlayer. The magnetic domains were recorded on the Si water using a standard optical recorder in the 'free running' mode because there are no pregrooves in the film. First, the whole thin window region was heated with a laser and magnetized uniformly in the positive z-direction, i.e. magnetized out-of-the-plane. Different tracks were written by accurate mechanical positioning of a lens used to focus the laser light as the external switching field was modulated. The bits were written with different switching field strengths. The vertical columns of bits in figs. 3a and 3b are, starting at the left, in the first column, 3 or 4 marker bits, and then successive columns of bits where the field strength used to write the bits was 0, 80, 120, 200, 300, 400 Oe, respectively. Prior to observation in SEMPA, the passivation layer was removed by sputtering with a 2 keV Ar ion beam while monitoring the composition with Auger electron spectroscopy.

The source of the magnetic contrast in the SEMPA images can be understood by analyzing the out-of-plane magnetization images shown in figs. 3a and b. In these SEMPA images, the grey levels indicate the magnitude of the magnetization along the z-direction, where white (black) is magnetization directed along the positive (negative) z-axis, i.e. out of (into) the page. In fig. 3a an image of thermomagnetically written bits in

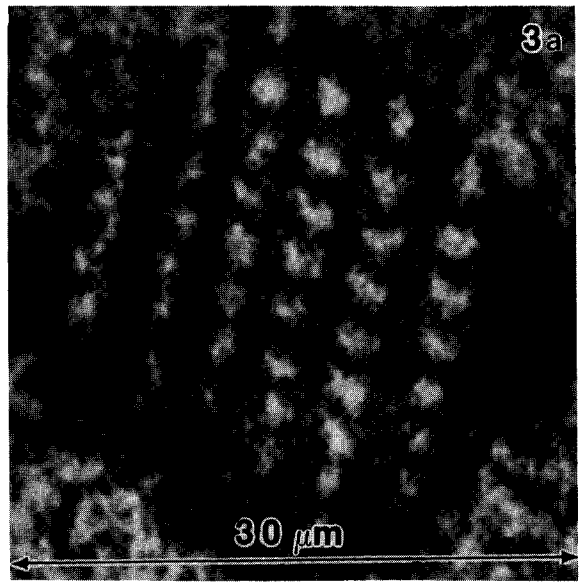

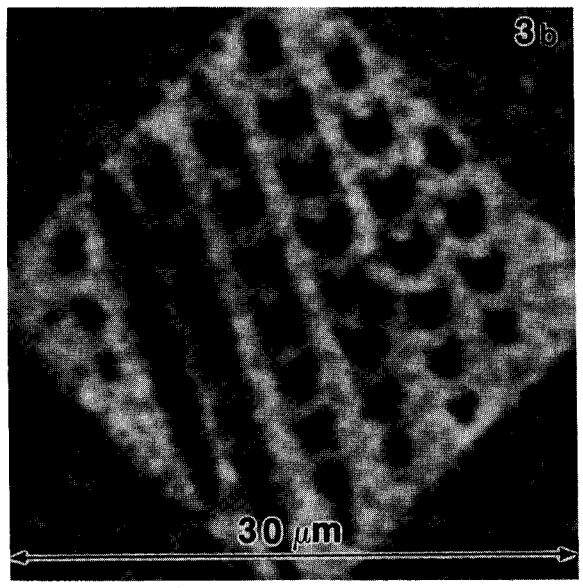

Fig. 3. The out-of-plane (z-component) component of the magnetization in MFM written bits in a 45 nm thick (a) $Tb_{30.0}Fe_{62.5}Co_{7.5}$ and (b) $Tb_{23.6}Fe_{67.6}Co_{8.8}$ film. The surface magnetization is normal to the plane for (a) and at 45° to the surface normal for (b).

$Tb_{30.0}Fe_{62.5}Co_{7.5}$ is shown. The Curie temperature for this sample is 450 K, and the compensation temperature is above the Curie temperature. This means that the Tb magnetic moments dominate the total magnetization for the ferrimagnet for all temperatures. As described previously, the whole thin film window was heated and magnetized in the positive z-direction, i.e. out-of-the-plane (out of the page in fig. 3a). Thus, the Tb moment which dominates the magnetization must point along the applied field direction and the Fe and Co moments which are anti-ferromagnetically coupled to the Tb moments must point anti-parallel to the applied field. Since the background within the thin film window in fig. 3a is black, the magnetization as measured in SEMPA is pointing in the negative z-direction, the same direction as the Fe and Co magnetic moments.

In fig. 3b an image of thermomagnetically written bits in $Tb_{23.6}Fe_{67.6}Co_{8.8}$ is shown. The Curie temperature for this sample is 473 K, and the compensation temperature is 213 K, below room temperature. This means that the Fe and Co magnetic moments dominate the total magnetization for the ferrimagnet for all temperatures at, and above, room temperature. Once again we can use the background magnetization within the thin film window to determine the magnetization orientation. In this case, since the Fe and Co magnetic moments dominate the magnetization, their magnetic moments must point along the applied field direction, along the positive z-axis, out-of-the-plane. The Tb magnetic moments must be oriented along the negative z-axis. Since the background within the thin film window in fig. 3b is white, the magnetization as determined by SEMPA is pointing in the positive z-direction, again in the same direction as the Fe and Co magnetic moments.

We conclude that the SEMPA signal (magnetization) originates in the transition metal subnetwork. This is the first observation of a ferrimagnetic system using SEMPA, and the first demonstration that the polarized secondary-electron cascade, which underlies the contrast in SEMPA, is dominated by the 3-d valence electrons from the transition metals in these magneto-optic alloys [8].

It is known that surface segregation and oxidation of the rare earth elements in rare-earth transition-metal alloys produced a variation in the magnetic behavior near the surface [23, 24]. This surface region may effect the signal to noise ratio of the read-back process as well as the domain formation process itself. Aeschlimann et al. [25, 26] have shown that an in-plane magnetic layer can exist at the surface even when the film is protected or in a UHV environment, and they proposed a simple model to describe the system. In their model [25, 26], the segregation and oxidation of the rare-earth produces a non-magnetic layer at the surface, a transition metal rich subsurface layer, followed by the bulk material. The transition metal rich subsurface layer exhibits a lower perpendicular anisotropy and a higher net magnetization.

SEMPA data for the two alloys of figs. 3a ($Tb_{30.0}Fe_{62.5}Co_{7.5}$) and 3b ($Tb_{23.6}Fe_{67.6}Co_{8.8}$) indicate the magnetization direction at the surface in nearly normal and at a 45° angle for these two alloys, respectively. The surface magnetization orientation is completely in the plane [8] for a $Tb_{21.2}Fe_{71.9}Co_{6.9}$ alloy. For the Tb rich sample ($Tb_{30.0}Fe_{62.5}Co_{7.5}$), the in-plane layer must be much thinner than the SEMPA probing depth, if it exists at all. For the low Tb concentration film ($Tb_{21.2}Fe_{71.9}Co_{6.9}$), the subsurface layer seems to be magnetized in the plane. Since the subsurface layer is not decoupled from the bulk magnetization, the subsurface layer must be thick enough, and possess enough in-plane anisotropy for the magnetization to rotate from out of plane in the bulk to in plane at the surface. For intermediate Tb concentrations ($Tb_{23.6}Fe_{67.6}Co_{8.8}$), the subsurface layer is not sufficiently thick, or the in-plane magnetocrystalline anisotropy is not sufficiently large to allow the magnetization to rotate completely from a normal orientation in the bulk to in plane at the surface, and hence the magnetization is oriented at a 45° angle to the surface.

4. Conclusion

We have shown that scanning electron microscopy with polarization analysis can be a useful tool for the quantitative analysis of micromagnetic structure at surfaces of thin films. We have used SEMPA measurements to verify micromagnetic models of 180° domain walls, and have thereby connected the SEMPA measurements of the surface magnetic microstructure to the micromagnetic structure in the interior of a film. The structure of cross-tie walls was shown to include two magnetic singularities, one elliptical and one hyperbolic type. The triangular structures visible in the cross ties is formed by the coupling of these two singularities. We illustrated how SEMPA can be used to study ferrimagnetic materials, and that the SEMPA image contrast in these materials is due to the transition metal subnetwork magnetic moments. Finally, we have shown that SEMPA can elucidate complex surface magnetic structure such as that formed in segregation layers in thin film magneto-optic materials.

Acknowledgements

This work was supported in part by the Office of Naval Research. M.A. wishes to thank the Schweizerische Nationalfonds for support. We wish to thank P. Ryan of Seagate Technology for supplying the permalloy films, and S. Klahn, F.J.A.M. Greidanus and M. Rosenkranz of Philips Research Laboratories for supplying the TbFeCo alloy samples. Finally, we would like to acknowledge the enormous contributions of M.H. Kelley and R. Freemire for image processing assistance.

References

[1] K. Koike, H. Matsuyama and K. Hayakawa, Scanning Micr. Intern. Suppl. 1 (1987) 241.
[2] J. Kirschner and H.P. Oepen, Phys. Bl. 44 (1988) 227.
[3] H.P. Oepen and J. Kirschner, Phys. Rev. Lett. 62 (1989) 819.
[4] G.G. Hembree, J. Unguris, R.J. Celotta and D.T. Pierce, Scanning Micr. Intern. Suppl. 1 (1987) 229.
[5] M.R. Scheinfein, J. Unguris, D.T. Pierce and R.J. Celotta, Phys. Rev. Lett. 63 (1989) 668.
[6] J. Unguris, M.R. Scheinfein, D.T. Pierce and R.J. Celotta, Appl. Phys. Lett. (1989) 2553.
[7] M.R. Scheinfein, J. Unguris, M.H. Kelley, D.T. Pierce and R.J. Celotta, Rev. Sci. Instrum. (1990) in press.
[8] M. Aeschlimann, M.R. Scheinfein, J. Unguris, F.J.A.M. Greidanus and S. Klahn, J. Appl. Phys. (1990) in press.
[9] J. Unguris, D.T. Pierce, A. Galejs and R.J. Celotta, Phys. Rev. Lett. 49 (1982) 72.
[10] M.R. Scheinfein, J. Unguris, J.L. Blue, K.J. Coakley, D.T. Pierce, R.J. Celotta and P.J. Ryan, Phys. Rev. B (1990) in press.
[11] A.E. LaBonte, J. Appl. Phys. 36 (1969) 1054.
[12] W.F. Brown, Micromagnetics (Kreiger, New York, 1978).
[13] A. Hubert, Phys. Stat. Sol. 32 (1969) 519, 38 (1970) 699.
[14] A. Aharoni, J. Appl. Phys. 37 (1966) 3271, J. Appl. Phys. 38 (1967) 3196; Phil. Mag. 26 (1972) 1473; Phys. Stat. Sol. (a) 18 (1973) 661; J. Appl. Phys. 46 (1975) 908, 914.
[15] B.D. Cullity, Introduction to Magnetic Materials (Addison-Wesley, Reading, MA, 1972) p. 433.
[16] R.J. Gambino, P. Chaudhari and J.J. Cuomo, in: Magnetism and Magnetic Materials (Denver, 1972), Proc. 18th Annual Conf. on Magnetism and Magn. Mat., AIP Conf. Proc. 18, eds. K.D. Graham Jr. and J.J. Rhyne (AIP, New York, 1973) p. 578.
[17] F.J.A.M. Greidanus, B.A.J. Jacobs, J.H.M. Spruit and S. Klahn, IEEE Trans. Magn. MAG-25 (1989) 3524.
[18] H-P.D. Shieh and M.H. Kryder, Appl. Phys. Lett. 49 (1986) 473.
[19] Y. Suzuki, N. Ota, M. Takahashi and S. Yonczawa, Appl. Phys. Lett. 55 (1989) 315.
[20] M. Hartman, B.A.J. Jacobs and J.J. Braat, Philips Tech. Rev. 42 (1985) 37.
[21] F. Tanaka, S. Tanaka and S. Suzuki, IEEE Trans. Magn. MAG-23 (1987) 2695.
[22] J.W. Jacobs and J.F. Verhoeven, J. Micr. 143 (1986) 103.
[23] P. Bernstein and C. Gueugnon, J. Appl. Phys. 55 (1984) 1760.
[24] S. Klahn, H. Heitmann, M. Rosenkrantz and H.J. Tolle, J. de Phys. 49 (1989) C8-1711.
[25] M. Aeschlimann, G.L. Bona, F. Meier, M. Stampanoni, A. Vaterlaus and H.C. Siegmann, Proc. Symp. on Magnetic Properties of Amorphous Metals, Benalmedena, Spain (May 1987) p. 70.
[26] M. Aeschlimann, G.L. Bona, F. Meier, M. Stampanoni, A. Vaterlaus, H.C. Siegmann, E.E. Marinero and H. Notarys, IEEE Trans. Magn. MAG-24 (1988) 3180.